



Origin and evolution of volatiles in the Central Europe late Variscan granitoids, using the example of the Strzegom-Sobótka Massif, SW Poland

Ł. Birski¹ · E. Słaby¹ · J. Domańska-Siuda²

Received: 6 September 2017 / Accepted: 26 June 2018 / Published online: 13 July 2018
© The Author(s) 2018

Abstract

The results of the new Electron Microprobe Analysis of apatite, hornblende and biotite crystals of the hornblende-biotite variety of the Strzegom-Sobótka granite indicate that these rocks experienced several phases during their evolution. During the first phase, the melting of the continental crust was caused by heating from basaltic magma. Nevertheless, the system was closed, and there is no evidence of the influence of any mafic component. The volatile compositions of apatite crystals recorded the signature of this phase. Afterwards, small quantities of mafic material were delivered into the crystallizing melt by ascending basaltic magma. The volatile composition of hornblende, together with dramatic changes in the F/Cl ratios between apatite and hornblende, indicates that the injection of mafic material occurred between the crystallization of both minerals. During the crystallization of hornblende, the system was closed. During the last episode, the volatile composition recorded by biotite indicates that the system opened again. This is represented by the decrease of Cl in the melt. Moreover, the estimated F concentrations in the melt range from ~2000 to ~3000 ppm and do not change significantly within the crystallization interval, whereas the Cl concentrations decreased from 1470–900 ppm at 829–768 °C to as low as 100 ppm at 710–650 °C, most likely due to the continuous exsolution of aqueous fluid from silicate melt or the crystallization of Cl-bearing minerals.

Keywords Volatiles · Strzegom-Sobótka massif · Granite · Variscides

Introduction

Volatiles such as H₂O, CO₂, S-species, halogens (such as F and Cl), and noble gases play enormous roles in igneous processes. They can influence magma viscosity, phase equilibria or crystallization temperatures. Furthermore, the injection of an external fluid phase can have strong effects on the generation of melts. The importance of volatiles in ascendancy of newly generated magmas towards the Earth's surface cannot be omitted. Since the solubility of volatiles dissolved in molten silicate phases increases with pressure, the ascent of

magmas to the surface with decreasing pressure causes bubbles to form. Therefore, studying volatiles may provide information about the role of fluids in igneous petrogenesis and the influence of volatiles on partial melting. Furthermore, to understand the overall evolution of igneous systems, we must quantitatively calculate and model the concentrations of volatiles during all stages of igneous petrogenesis. The most common volatile is H₂O. Most silicic magmas contain 2 to 4 wt. % water (Whitney 1988). Furthermore, OH-bearing minerals (i.e., apatite, amphibole, biotite, and muscovite) can be commonly found in many magmatic rocks (e.g., Zhang et al. 2012; Teiber et al. 2014; Bao et al. 2016). The second-most abundant volatile compound is CO₂. This component causes the polymerization of the melt and therefore changes the temperature at which the melt begins to crystallize (Maksimov 2009). The presence of sulfur is obvious. It is particularly important for understanding the genesis of many ore deposits (Mungall et al. 2015). Moreover, the presence of common sulfides and infrequent sulfates additionally confirms the importance of sulfur (Huston et al. 2011). In the vast majority of silicate melts, the concentrations of halogens, such as F and Cl, rarely

Editorial handling: M.A.T.M. Broekmans

✉ Ł. Birski
l.birski@twarda.pan.pl

¹ Institute of Geological Sciences, Polish Academy of Sciences, Research Center in Warsaw, Twarda 51/55, 00-818 Warsaw, Poland

² Institute of Geochemistry, Mineralogy and Petrology, Warsaw University, Żwirki i Wigury 93, 02-089 Warsaw, Poland

exceed 5,000 ppm. Regardless, they play an important role in the evolution of magmatic systems and their associated ore deposits (Hedenquist and Lowenstern 1994), as well as in the transport of metal in magmatic systems (Aiuppa et al. 2009). Furthermore, they are components of volatile-bearing minerals, such as apatite, biotite and amphibole, and they can occasionally create their own minerals, e.g., fluorite or sylvite (Baker et al. 2005).

The Strzegom-Sobótka Massif (SSM) was emplaced in the Late Carboniferous – Early Permian by four magmatic pulses associated with a gradual but significant increase in magma temperature of at least 140 °C, from c. 720 to 860 °C; this event has been dated to 305–294 Ma. This progressive heating, which followed the cessation of Variscan orogenesis, can be explained by the input of heat into the crust contributed from ascending basaltic magmas. Therefore, the origin of the SSM is thought to be related to the bimodal volcanism that was widespread across the Sudetes Mountains and the northern Variscan foreland (Awdankiewicz et al. 2010). The formation of basaltic magmas was activated by the decompressional melting of the lithospheric mantle (Wilson et al. 2004). Afterwards, it provided thermal influx into the lower crust, causing its melting. Therefore, the origin of SSM cannot be associated with the Variscan cycle (Turniak et al. 2014). The emplacement of the SSM, together with the occurrence of bimodal volcanism, signaled the change from a convergent to an extensional tectonic regime and the commencement of lithospheric thinning beneath Central Europe (Turniak et al. 2014).

The Variscan melts are very well studied, and we have extensive knowledge about their age, composition and origin. Unfortunately, there is a lack of information about the composition of their volatiles. Therefore, in this study, an attempt was made to measure the concentrations of volatiles in amphibole, biotite and apatite from the SSM. Additionally, concentrations of Cl, F and H₂O in felsic melt were also calculated. We tried to determine the characteristics of the volatile components, as well as the source or sources of volatiles in the magma. It was possible to determine crystallization parameters, such as the temperature and pressure of crystallization. Chemical analyses of volatile-bearing minerals were used to make all calculations.

Geological setting

The SSM is located within the Variscan internides of the Sudetes at the NE margin of the Bohemian Massif in the central region of the Fore-Sudetic block (Fig. 1). It is emplaced into various, mostly allochthonous lithological units that were deformed and metamorphosed during the Variscan epoch. The SSM is composed of various post-kinematic granitoids. The massif is predominantly covered by Permian,

Mesozoic and Cenozoic formations. The SSM is elongated in the SE-NW direction, and it has an approximate length of 50 km and a maximal width of 12 km. The granitoid pluton is divided into its eastern and western parts by the Strzegom-Świdnica dislocation. The SSM is surrounded by many kind of units, which are mostly mafic, ultramafic, metamorphic and sedimentary rocks. The Góry Sowie massif borders the SSM on the southeast and is mainly composed of gneisses and migmatites, which are subordinately accompanied by mafic and ultramafic rocks as well as small granulitic bodies (Oliver et al. 1993; Brueckner et al. 1996; Kröner 1998). On its eastern end, the SSM contacts with mafic and ultramafic rocks of the Ślęza massif, i.e. gabbros, serpentinites, amphibolites and metavolcanites (Pin et al. 1988; Kryza and Pin 2002), whereas on the northwestern side, the granitic intrusion borders with the Sudetic boundary fault, which separates the massif from the metamorphic rocks of the Kaczawskie Mts. On the northern and southeastern sides, the SSM is accompanied by the Early Paleozoic micaceous, sericitic, chloritic and quartzite schists, that are locally intercalated by dolomite and greywacke-argillaceous schists, diabases and quartzites. They are deeply hidden under the Cenozoic deposits (Majerowicz 1972).

Petrology of the SSM

Four rock types have been described in the SSM (Kural and Morawski 1968; Maciejewski and Morawski 1970, 1975; Majerowicz 1972; Puziewicz 1985, 1990), namely, hornblende-biotite granite and biotite granite, which occur in the western part, and two-mica granite and biotite granodiorite, which mainly appear in the eastern part (Fig. 2). All groups can be clearly distinguished by their petrography and geochemical and isotopic compositions (Puziewicz 1985, 1990; Pin et al. 1988, 1989; Domańska-Siuda and Słaby 2003, 2004, 2005; Domańska-Siuda 2007).

All samples of the hornblende-biotite variety of the Strzegom-Sobótka granite were collected from the western part of the massif (Fig. 2). All sampling localities have been summarized in Table 1.

Hornblende-biotite granite is the dominant type of granite in the western part of the Strzegom-Sobótka Massif. This granite is an equigranular, medium- to coarse-grained light grey rock with non-directional fabric; locally, it has porphyritic texture. Its main constituents are K-feldspar, hornblende, biotite, quartz and zoned plagioclase (An<30%) (Fig. 3). Its accessory minerals include zircon, apatite, allanite, sphene, rutile, monazite, xenotime and opaque minerals (Fig. 3). Furthermore, hornblende-biotite granite often contains mafic microgranular enclaves, xenoliths, schlieren and aplite veins (Puziewicz 1985; Domańska-Siuda 2007).

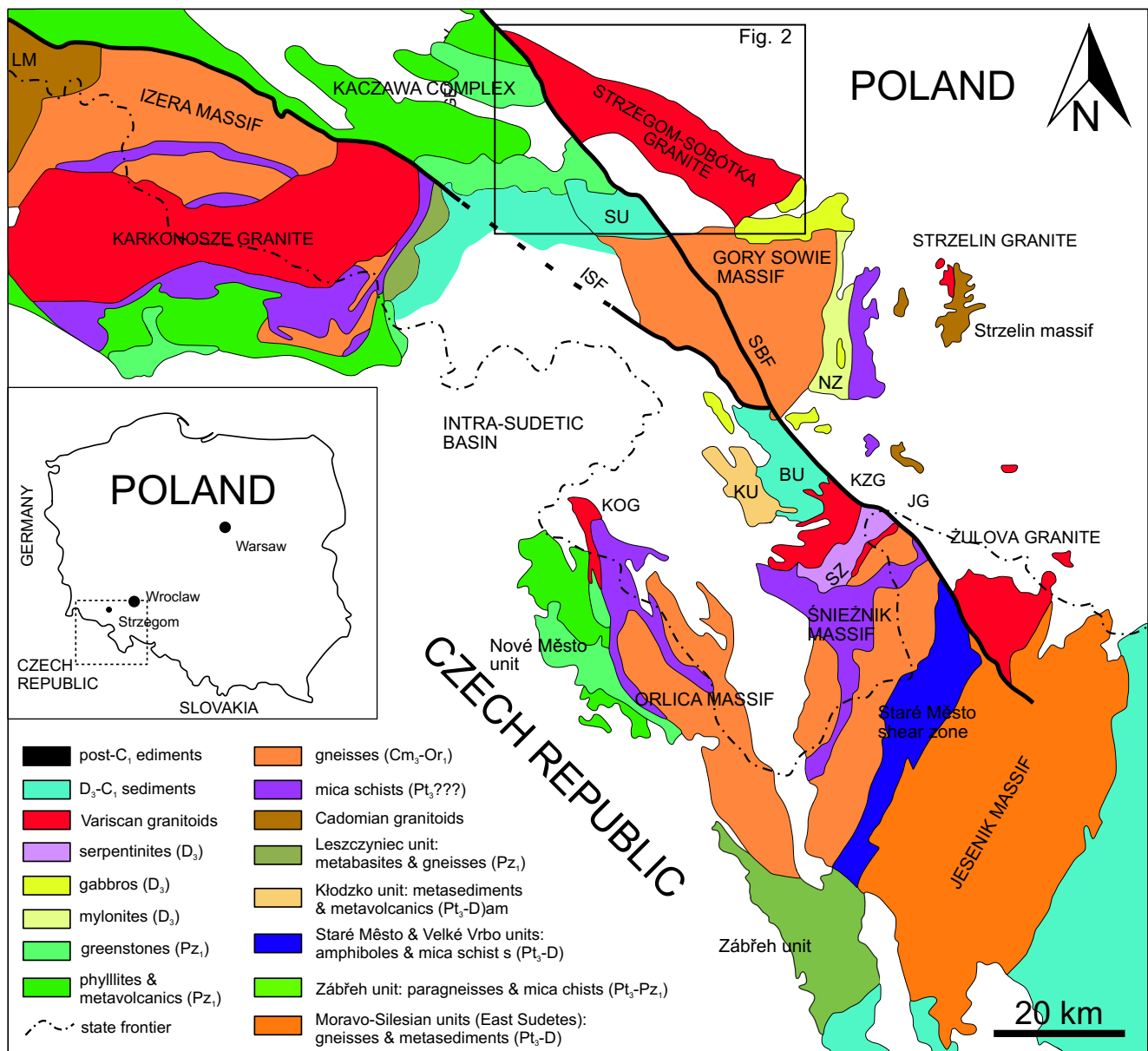


Fig. 1 Geological sketch map of the Sudetes. Abbreviations: BU—Bardo Sedimentary unit; ISF—Intra-Sudetic fault; JG—Jawornik granite; KOG—Kudowa-Oleśnice granite; KU—Kłodzko metamorphic unit; KZG—Kłodzko—Złoty Stok granite; LM—Lusatian Massif; NZ—Niemcza shear zone; OSD—Orlica-Śnieżnik dome; SU—Świebodzice

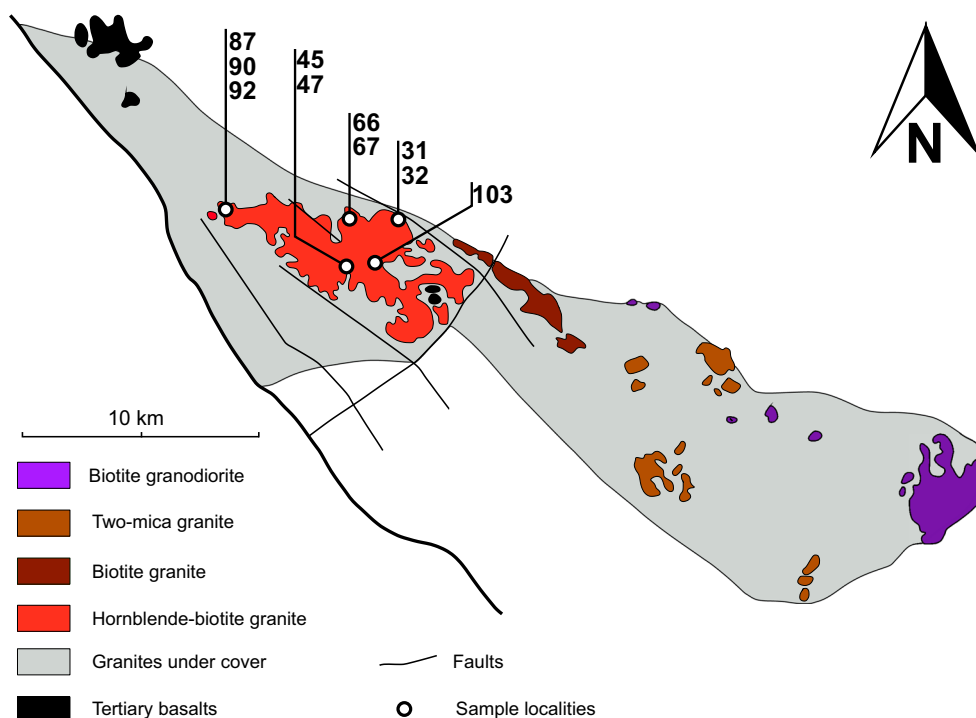
sedimentary unit; SBF—Sudetic boundary fault; SZ—Skrzynka shear zone. Age assignments: Pt—Proterozoic; Pz—Palaeozoic; Cm—Cambrian; Or—Ordovician; D—Devonian; C—Carboniferous; 1—Early; 2—Middle; 3—Late. Modified after Aleksandrowski et al. (1997)

The hornblende-biotite granite contains 72.1–75.6 wt.% SiO₂, and it is predominantly metaluminous, as its alumina saturation index values range from 0.83 to 1.04. Its SiO₂ contents exhibit negative linear correlations with Al₂O₃, Fe₂O₃, MgO, CaO and Na₂O. K₂O is not correlated with SiO₂. The trends defined by TiO₂, MnO, and P₂O₅ are rather poorly visible. The hornblende-biotite granite has calc-alkalic and alkali-calcic characteristics. Furthermore, it is ferroan and magnesian (Borkowska 1957; Majerowicz 1972; Puziewicz 1990; Domańska-Siuda 2007). The imprecise age of the hornblende-biotite granite estimated by Pin et al. (1989) (Rb–Sr

method, whole rock) was 278 ± 7 Ma. Newer zircon Pb-evaporation dating yielded a considerably older age of 302.9 ± 2.2 Ma (Turniak et al. 2005). Furthermore, dating molybdenite using the Re–Os method yielded estimated ages of 296 ± 2 to 298 ± 1 Ma (Mikulski and Stein 2005). The K–Ar cooling ages of the hornblende-biotite granite are 291.0 ± 4.4 Ma and 298.7 ± 5.2 Ma (Turniak et al. 2007). SHRIMP U–Pb zircon dating of the hornblende-biotite granite yielded ages of 297.7 ± 2.2 Ma and 297.1 ± 3.0 Ma (Turniak et al. 2014).

Apatite is an accessory mineral in the hornblende-biotite granite. It appears as inclusions in light minerals but can also

Fig. 2 Geological sketch map of the Strzegom-Sobótka Massif showing locations of dated samples. Simplified after Turniak et al. (2014)



be observed in biotite or hornblende. It mostly forms automorphic, elongated crystals that are up to 0.3 mm long (Fig. 3).

Biotite is the most common mafic mineral in the hornblende-biotite granite. It forms mostly subhedral to anhedral plates that are up to 2 mm long and are sometimes grouped into aggregates (Fig. 3). It exhibits pale straw yellow to dark brown pleochroism. Often, biotite contains inclusions of zircon (with pleochroic halos), allanite, ilmenite, apatite and rutile. Locally, biotite is replaced by chlorite-group minerals; this mainly occurs along the cleavage planes, fractures and marginal regions of grains. Moreover, biotite itself can be found pseudomorphosed after amphibole, even exhibiting its primary prismatic shape. The Fe/(Fe+Mg) ratios of biotite

range from 0.73–0.85. Biotite also contains 2.32–2.62 atoms of Al^{IV} pfu (per formula unit), which classifies it in between the siderophyllite and annite mixed-crystals series (Domańska-Siuda 2007).

Amphibole is a relatively minor compound, and it occurs in variable amounts. This mineral forms subhedral to nearly euhedral crystals (Fig. 3). Its pleochroism is plain green. Locally, amphibole is replaced by biotite. Its $A(Na+K+2Ca)$ apfu range from 0.40 – 0.61, whereas $C(Al+Fe^{3+}+2Ti)$ apfu from 1.08 – 1.40. According to classification of Hawthorne et al. (2012) amphibole from the hornblende-biotite granite can be classified as magnesiohornblende and pargasite.

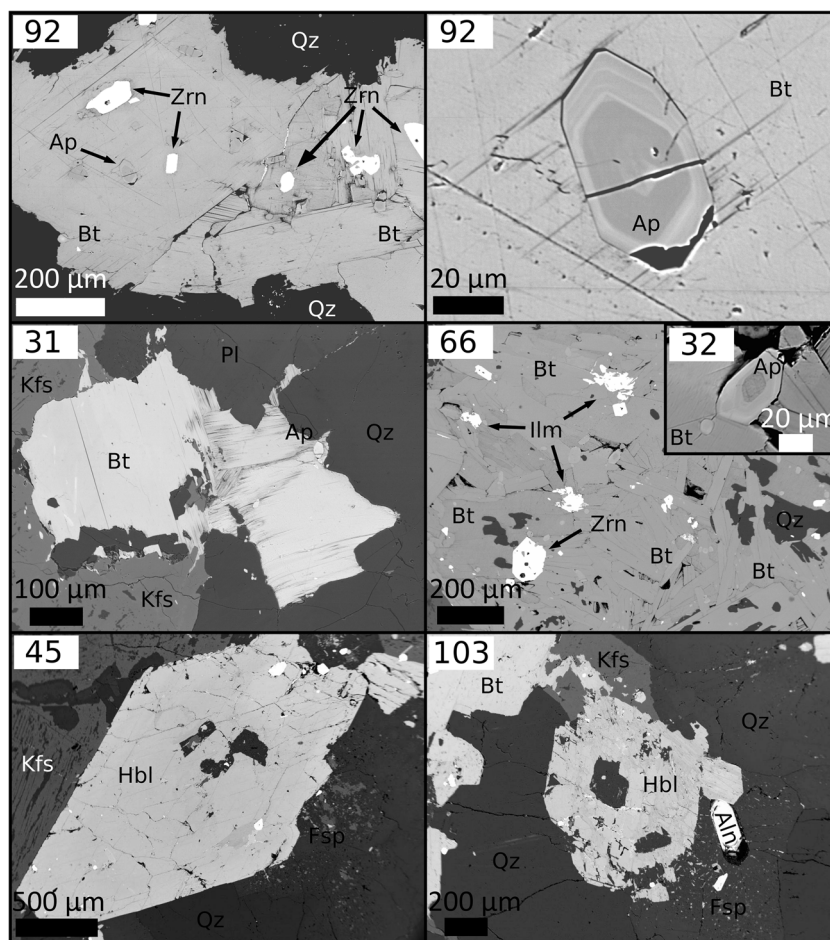
Pin et al. (1988) and Pin et al. (1989) first proposed that four magmatic batches were involved in the genesis of the SSM rocks. Furthermore, they suggested that the origin of the SSM might be related to the widespread bimodal volcanism that occurred across the Variscan foreland; they also suggested that mantle input was present in the western part of the SSM.

In the eastern part of the SSM, a two-mica granite crystallized from magmas that are of a crustal origin and do not record any mantle contributions. This is suggested by its Sr_i value, which is 0.7050 (Pin et al. 1989), and its ϵ_{Nd} values, which range from c. –2.9 to –6.3 (Pin et al. 1988). Furthermore, this rock has peraluminous ($ASI > 1$) and dominantly calc-alkalic ($Al_2O_3 > Na_2O + K_2O$) characteristics. The two-mica granite comprises only xenoliths and restite (Majerowicz 1972). This two-mica granite was emplaced at 304.8 ± 2.7 Ma (Turniak et al. 2014). Furthermore, it records the lowest zircon saturation temperature (TZr) of c. 720 °C.

Table 1 Sampling locations and apatite saturation temperatures (ASTs) (Harrison and Watson 1984) of apatite from the hornblende-biotite granite

Sample	Quarry	Locality		ASTs
31	Wieśnica	N: 51°00'14"	E: 16°18'29"	892
32	Wieśnica	N: 51°00'14"	E: 16°18'29"	892
45	Borów	N: 50°59'05"	E: 16°15'24"	910
47	Borów	N: 50°59'05"	E: 16°15'24"	910
66	Zimnik	N: 51°00'39"	E: 16°14'16"	981
67	Zimnik	N: 51°00'39"	E: 16°14'16"	901
87	Paszowice	N: 51°00'26"	E: 16°14'51"	894
90	Paszowice	N: 51°00'26"	E: 16°14'51"	894
92	Paszowice	N: 51°00'26"	E: 16°14'51"	894
103	Kostrza Kwarce	N: 50°58'39"	E: 16°15'49"	986

Fig. 3 Backscattered electron images of typical mineral assemblages of granitic rocks of SSM. Abbreviations: Aln – Allanite, Ap – Apatite, Bt – Biotite, Fsp – Feldspar, Hbl – Hornblende, Ilm – Ilmenite, Kfs – K-feldspar, Pl – Plagioclase, Qz – Quartz, Zrn – Zircon (Whitney and Evans 2010)



(Turniak et al. 2014). According to Barbarin (1999), this two-mica granite is classified as an MPG (muscovite-bearing peraluminous granitoid).

The influence of mafic material is first visible in case of the biotite granodiorite. This rock is rich in enclaves (Domańska-Siuda 2007). Its Sr_i value is 0.7055 (Pin et al. 1989), whereas its ϵ_{Nd} values range from c. -2.3 to -2.7 (Pin et al. 1988). Its Sr ratios and ϵ_{Nd} values deviate from the characteristic signatures of KCG (K-rich calc-alkaline granitoids) and ACG (amphibole-rich calc-alkaline granitoids). Furthermore, this rock does not contain amphibole, pyroxene, muscovite or cordierite – all minerals that are characteristic of both granitoid types. On the other hand, the biotite granodiorite contains mafic microgranular enclaves (MMEs), which are characteristic of both of these types of granitoids. Pin et al. (1988) explained the ambiguous characteristics of this biotite granodiorite as resulting from its mixing with a small amount of mafic material with low initial Nd/Sm and Rb/Sr ratios. Furthermore, the age of the biotite granodiorite falls between 301.9 ± 3.6 and 297.9 ± 3.7 Ma, and its zircon saturation temperature is 740 – 780 °C (Turniak et al. 2014).

Pin et al. (1989) and Domańska-Siuda (2007) analysed the hornblende-biotite granite and obtained Sr_i values of 0.7098

and 0.7096, respectively. Furthermore, Pin et al. (1988) and Domańska-Siuda (2007) obtained ϵ_{Nd} values of -4.2 and -3.4 , respectively. The hornblende-biotite granite commonly contains MMEs and rarely contains xenoliths. According to the classification of Barbarin (1999), most of the features of the hornblende-biotite granite indicate that it belongs to the KCG (K-rich calc-alkaline granitoids) type. Furthermore, the age of the hornblende-biotite granite is 297.1 ± 3.0 Ma, and its calculated TZr values range from 800 – 860 °C (Turniak et al. 2014). These data indicate that the hornblende-biotite is of mixed origin. In general, crustal- and mantle-derived components are expected to be involved in the formation of KCG-type granites. Although granitic melt mixed with mafic melt, the influence of the mafic melt was negligible due to its insignificant volume. Therefore, the final evolution of the hornblende-biotite granite was the result of the interaction between crustal melt and a small quantity of mafic melt, which was probably generated from the metasomatized mantle (Pin et al. 1989; Puziewicz 1990; Domańska-Siuda and Słaby 2003, 2004, 2005). Due to the minor influence of magma mixing, the magmatic evolution of the hornblende-biotite granite was mostly controlled by the fractional crystallization of plagioclase, biotite, and amphibole.

The last observed in the SSM type of granite variety is biotite granite. The mineral, chemical and isotopic compositions of this rock are similar to those of the hornblende-biotite granite. The most significant difference is its lack of amphiboles and MMES or xenoliths, which are often visible in the hornblende-biotite granite (Kural and Morawski 1968; Majerowicz 1972). Biotite granite has s-type characteristic (Pin et al. 1988, 1989). Its Sr_i value is 0.7082 (Pin et al. 1989), and its ϵ_{Nd} value is -4.5 (Pin et al. 1988). These values are similar to those of the hornblende-biotite variety. Small differences between granitoids can be explained by the crystallization of the hornblende-biotite variety from slightly more differentiated melts than the less evolved biotite granite variety (Maciejewski and Morawski 1975; Pin et al. 1989). Furthermore, the crustal component was more significant in the case of the biotite granite.

Analytical procedures

Sampling

The main idea of our sampling was to reflect the character of the hornblende-biotite variety of the SSM and its petrologic and geochemical characteristic. Therefore, the analyzed samples cover all the complexity and local diversity of hornblende-biotite variety (Fig. 2, Table 1). We tried to select samples that were visually the most representative, free of secondary alterations and as far as possible from the MMEs. In most cases, from more than one place in the single outcrop or quarry. Thin sections (30 μ m thickness) were prepared from all collected samples.

Electron Microprobe Analysis (EMPA)

The chemical compositions of biotite, amphibole and apatite were investigated using the CAMECA SX-100 electron microprobe equipped with four wavelength spectrometers at the Electron Microprobe Laboratory of the Inter-Institute Microanalytical Complex for Minerals and Synthetic Substances, Institute of Geochemistry, Mineralogy and Petrology, University of Warsaw. Prior to the analyses, the thin sections were coated with a 20 nm thick carbon film to prevent charging under the electron beam. In order to minimize the known potential with migration of F, Cl (eg. Stormer et al. 1993) and Na quantitative spot analyses of biotite, amphibole and apatite were conducted following the modified measurement protocol of Slaby et al. (2016). The measurement conditions were as follows: a beam current of 10 nA, an accelerating voltage of 15 kV, a counting time of 20 s and spot size of 8 μ m. The following standards were used: albite (Na); diopside (Mg, Si, Ca); wollastonite (Si, Ca); orthoclase (K, Al); haematite (Fe); rhodochrosite (Mn); apatite (P, F); phlogopite (F); barite (S, Ba); rutile (Ti); synthetic strontium titanate (Sr); Y – Al

garnet (Y); synthetic NiO (Ni); synthetic lanthanum hexaboride, LaB₆ (La); synthetic cerium(III) ultraphosphate, CeP₅O₁₄ (Ce); synthetic neodymium gallate, NdGaO₃ (Nd); synthetic chromium(III) oxide, Cr₂O₃ (Cr); and tugtupite (Cl). The background counting times were set to half of the respective peak counting times. The analytical errors for analyzed elements depend on the absolute abundances of each element. Relative errors are estimated to be <1% at the >10 wt% level, about 1% at the 5–10 wt% level, 1–5% at the 1–5 wt% level, 1–10% at the 0.1–1 wt% level, and 10–20% at the <0.1 wt% level. Detection limits for the apatite were between 150–650 ppm for main and trace elements, approximately 900 ppm for analyzed REE except La (2700 ppm), whereas for the biotite and amphibole between 150–850 ppm except Ti in biotite (2400 ppm). The Armstrong PRZ correction algorithm for oxides was used for data processing. The obtained results were analysed using several modelling sheets. Amphibole analyses were recalculated using the Amp – TB spreadsheet (Ridolfi et al. 2010). Additionally, the chlorine and fluorine concentrations in melts were calculated. For amphiboles, the methods approved by Sato et al. (2005) and Zhang et al. (2012) were used. The models used to estimate the concentrations of volatiles in biotite were those of Munoz (1992) and Zhang et al. (2012). For apatite, the models suggested by Webster et al. (2009) were used. It was also possible to establish apatite saturation temperatures (Harrison and Watson 1984).

Background of models estimating melt compositions and parameters of crystallization

Estimation of the P, T conditions of melt crystallization

Whole-rock analyses were used to estimate apatite saturation temperatures (ASTs). These ASTs were calculated using the following equation of Harrison and Watson (1984):

$$\ln D_p^{apatite/melt} = [(8400 + (SiO_2 - 0.5) \cdot 26400) / T] - [3.1 + (12.4 \cdot (SiO_2 - 0.5))],$$

where SiO₂ is the weight fraction of silica in the melt. According to the authors, this relationship appears to be valid between 45 wt.% and 75 wt.% SiO₂ and up to 10 wt.% H₂O. This equation is useful in the temperature range of 850 to 1500 °C. The silica and P₂O₅ contents of the model were obtained from personal communication with J. Domańska-Siuda.

Unfortunately, there are no geothermometers dedicated to estimating the crystallization conditions of magmatic biotite. Nevertheless, it can be assumed that most biotite likely crystallized or was equilibrated at a near-solidus temperature of approximately 680 °C (Naney 1983).

To determine the P-T conditions of amphibole crystallization, the Amp – TB spreadsheet developed by Ridolfi et al. (2010)

was used. Its limitations are 1064–766 °C and 73–1000 MPa. Furthermore, the Amp – TB spreadsheet provides estimations of crystallization depth. Moreover, the results can be easily plotted onto stability curve diagrams. For temperatures, this method yields errors of approximately ± 22 °C. Unfortunately, the errors for high-Al amphiboles that crystallized in the mantle are much larger (± 55 °C). According to Ridolfi et al. (2010), aluminium content exhibits the best correlation with pressure. The calculated σ_{est} value is 54 MPa, but it strongly decreases at 39 MPa, where the average relative error is $\pm 14\%$. At 1 GPa, the relative error can be as high as 33%. Furthermore, near the P–T stability curve, the error is 8–11%; in contrast, for lower-T magmas, this uncertainty increases up to 24%, which is consistent with the depth uncertainties of 0.40 km at 90 MPa (c. 3.4 km) and 3.95 km at 800 MPa (c. 30 km).

Furthermore, water contents in melt were estimated using the model of Holtz et al. (2001):

$$S_{H_2O} = 2.859 \cdot 10^{-2} \cdot P - 1.495 \cdot 10^{-3} \cdot P^{1.5} + 2.702 \cdot 10^{-5} \cdot P^2 + 0.257 \cdot P^{0.5},$$

where S_{H_2O} is the water solubility of silicate melts in wt.%, and P is pressure in MPa. According to the authors, this equation was proposed for rhyolitic melts at c. 800 °C. Its estimated error is ± 0.05 wt.%. Furthermore, this model was proposed for pressures ranging from 0.3 – 8 kbar.

Estimation of F and Cl concentrations in melt

Several experimental and theoretical studies have investigated the partitioning behaviour of F and Cl in apatite–melt–fluid systems (Zhu and Sverjensky 1991, 1992; Piccoli and Candela 1994; Piccoli et al. 1999; Mathez and Webster 2005; Webster et al. 2009; Zhang et al. 2012). As demonstrated by the experiments of Mathez and Webster (2005) and Webster et al. (2009), the partitioning of F and Cl in the apatite–melt–fluid system can be treated as a function of melt composition. For felsic melts, the equation proposed by Webster et al. (2009) can be used. Using rhyodacitic melts (70.4 wt.% SiO₂), the authors were able to determine partition coefficients for fluorine between apatite and melt. This equation is defined as follows:

$$X_{FAp}^{Ap} = 3.02 \cdot W_F^m + 0.12$$

where W_F^m is the fluorine concentration in the melt and X_{FAp}^{Ap} is the concentration of fluorite in the X-site, in which the sum of F+Cl+OH = 1. This partitioning model should be valid for apatite–melt systems with F concentrations of >300ppm. Furthermore, it can be noted that the effect of temperature in these systems is negligible. Unfortunately, the concentrations of chlorine in apatites from the SSM are very low, and they are frequently below the detection limit. Therefore, it is impossible to determine the concentrations of Cl in the granitic melt of the SSM.

Unfortunately, there is only one model that quantitatively describes Cl in the melt on the basis of amphibole composition. Sato et al. (2005) determined the reaction between amphibole and dacitic melt at conditions of 2–3 kbar and 800–850 °C. Thus, Zhang et al. (2012) rewrote this equation to express the Cl–OH partition coefficient as a function of the Mg# of amphibole, which has the form: $\log(Cl/OH)_{\text{melt}} = (Cl/OH)_{\text{Amp}} - 3.74 + 1.5 \times Mg + 0.0027 \times T$,

where $(Cl/OH)_{\text{melt}}$ and $(Cl/OH)_{\text{Amp}}$ are the molar ratios in the melt and amphibole, respectively, Mg# is Mg/(Mg+Fe) and T is temperature in Kelvin. The OH mole fraction needed for this calculation can be acquired based on the calculation of the H₂O species in silicate melt. This equation, according to Zhang et al. (2012), has the following form:

$$[OH] = 2A + \left(8A + K - 2AK + \sqrt{K} \cdot \sqrt{16A + 16A^2 + K - 4AK + 4A^2K} \right) / (K - 4),$$

where A is the total water in moles and K is a temperature-dependent coefficient that can be expressed, according to Nowak and Behrens (2001), as follows:

$$K = 27,98 \times e^{-4210/T}.$$

Based on the equation of Sato et al. (2005), Zhang et al. (2012) established a similar equation that is applicable to the concentration of fluorine in melt. This equation is:

$$\log(F/OH)_{\text{melt}} = (F/OH)_{\text{Amp}} + 0.19 - Mg.$$

In this equation, the effect of temperature is neglected. The negative value of Mg# (Mg/(Mg+Fe)) is consistent with the fact that Mg promotes the incorporation of F (i.e., the Fe–F avoidance rule, according to Munoz (1984) and Mason (1992)).

Few studies have been devoted to the experimental calibration of the distribution of F and Cl between biotite and its crystallization environment. Biotite has mainly been treated as a monitor for investigating volatile evolution in magmatic–hydrothermal systems (e.g., Munoz 1984; Zhu and Sverjensky 1991, 1992; Finch et al. 1995; Coulson et al. 2001; Harlov and Forster 2002). The main reason for this is the strong tendency of biotite to recrystallize (Icenhower and London 1995), yet in case of this study only magmatic biotites without any traces of recrystallization have been analyzed. Additionally, it may record only the latest, subsolidus values of volatile contents in coexisting vapor (e.g., Munoz (1984)). To estimate the F concentrations in granitic melt, the model of Icenhower and London (1997) can be used. This equation has the following form:

$$D_F^{Bt/E} = W_F^{Bt} / W_F^m = 10.08 \times Mg - 1.08$$

where W_F^{Bt} and W_F^m are the F concentrations in biotite and melt, respectively, and Mg# is Mg/(Mg+Mn+Fe), where all values are calculated as atoms pfu. Furthermore, Icenhower

and London (1997) managed to determine the partition coefficient of chlorine between biotite and melt. For biotite crystals with Mg# values of approximately 0.28, the authors obtained two values of $D_C^{Bt/E}$, namely, 2.97 and 6.25. Although the Mg# values of the biotite crystals in this study are similar to or lower than the Mg# values used in the study of Icenhower and London (1997), both values of $D_C^{Bt/E}$ (2.97 and 6.25) were used in these calculations. In both scenarios, according to the authors, the influence of pressure can be neglected. According to Icenhower and London (1997), this model is suitable for granitic melts.

Results

The chemical compositions of apatite crystals from all samples were determined using EMP analysis. Chemically, the apatite crystals in all of the samples are fluorapatites. The results of their compositions are reported in Table 2. These electron microprobe analyses demonstrated the lack of significant differences in the compositions of all samples. The mean formula of the apatite crystals from the hornblende-biotite granite is $(Ca_{4.91}Fe_{0.03}Na_{0.02}Mn_{0.03}Y_{0.02}REE_{0.03})_{5.04}(P_{2.95}Si_{0.04})_{2.98}O_{12}(F_{0.97}OH_{0.03})_2$. Their measured fluorine concentrations range from 3.00–3.80 wt.%, therefore according to classification of Pasero et al. (2010) apatite from the hornblende-biotite granite is fluorapatite. Their OH contents were calculated assuming that the X-site is completely filled, i.e., $F+Cl+OH=2$. Applying this normalization scheme yields OH components ranging from 0–22 mole%, which equals up to 0.54 wt.% H₂O. The concentrations of Cl in the apatite crystals of the hornblende-biotite variety of the SSM are very low and close to detection limits, up to 0.07 wt.% Cl. Furthermore, their F/Cl ratios range from 96–6900 (Table 3). The analysed fluorapatite crystals contain Fe, Mn, Y, Si and REE. As calculated from the equation of Harrison and Watson (1984), the apatite saturation temperature is 910–892 °C (Table 1). Furthermore, the concentrations of fluorine in melt, as calculated according to the equation of Webster et al. (2009), range from 2200–3000 ppm (Table 3). Since the content of Cl in apatite is close to the detection limit, it was not possible to estimate Cl concentrations in melt using apatite.

Amphibole crystals were observed and analysed in samples 47 and 102. Their mean analyses are presented in Table 4. The mean formula of the amphibole crystals from the hornblende-biotite granite from the western part of the Strzegom-Sobótka Massif is $(K_{0.22}Na_{0.31})_{0.53}(Na_{0.28}Ca_{1.72})_2(Mn_{0.08}Fe^{2+}_{2.87}Mg_{1.05}Fe^{3+}_{0.68}Ti_{0.23}Al^{VI}_{0.10})_5(Al^{IV}_{1.49}Si_{6.51})_8O_{22}(F_{0.19}Cl_{0.06}OH_{1.75})_2$. Their measured fluorine concentrations range from 0.08–0.54 wt.%, which are equal to 0.04–0.27 F atoms pfu. OH content in amphibole was calculated assuming that the X-site is completely filled, i.e., $F+Cl+OH=2$;

these OH components range from 1.66–1.90 OH pfu. Chlorine concentrations in amphibole range from 0.02–0.06 Cl atoms pfu. Furthermore, their F/Cl ratios range from 1.5–5. Crystallization temperatures of amphiboles range from 768–829 °C, with an error of 22 °C, whereas the pressure dropped from 223 ± 56 to 144 ± 36 MPa during crystallization (Table 5). Furthermore, the H₂O content during hornblende crystallization was 5.5–6.5 wt.% (Table 5). The concentrations of fluorine and chlorine in melt, as calculated according to the equations of Sato et al. (2005), have values of 3000–1000 and 1470–900 ppm, respectively (Table 5).

Biotite crystals from all samples were measured using EMPA. Their average spot compositions are presented in Table 6. The mean formula of the biotite crystals from the hornblende-biotite granite from the western part of the SSM is $(K_{1.93})(Mg_{0.91}Mn_{0.07}Fe^{2+}_{4.09}Ti_{0.46}Al^{(VI)}_{0.16})_{5.69}(Al^{(IV)}_{2.41}Si^{(IV)}_{5.59})_{8.00}O_{22}(F_{0.01}Cl_{0.00}OH_{1.98})_2$. There are no significant compositional differences between the measured biotite crystals. Their measured fluorine and chlorine concentrations range from 0.04–0.56 and 0.06–0.29 wt.%, with average values of 0.26 and 0.13 wt.%, respectively. The OH component, computed on the assumption that $F+Cl+OH=2$, ranges from 1.973–1.997 atoms pfu. Furthermore, their F/Cl ratios range from 1–24. The concentrations of fluorine in melt, as calculated using the equation of Icenhower and London (1997), range from 3200–600 ppm. Furthermore, the calculated Cl concentrations in melt, based on $D_C^{Bt/E}$ values of 2.97 and 6.25, are 1000–200 and 500–100 ppm (Table 7), respectively.

Discussion

P-T conditions and water content in melt

Due to the common lack of minerals that might be used as geobarometers, it is not easy to estimate the pressure of crystallization of granitic rocks. The rocks of the SSM are not the exceptions to this rule. However, there are methods that can be used to estimate the pressure of rock crystallization. First, it is possible to obtain pressure from surrounding rocks that were formed during contact metamorphism and might contain minerals that can be used as indicators of pressure. The presence of andalusite in the SSM contact aureoles (Majerowicz 1972) indicates that the pressure was not greater than 380 MPa, which represents a depth of less than 15 km (Holdaway 1971). Furthermore, in the neighbouring area, tourmaline-andalusite aplite is present. This rock may be genetically associated with the hornblende-biotite granite (Puziewicz 1981). Andalusites of magmatic origin are stable at pressures ranging from 100–200 MPa (Pichavant and Manning 1984). That implies that the Strzegom-Sobótka granite crystallized at relatively low pressures. Moreover,

Table 2 Main element oxide contents of selected apatite grains from the SSM granitoids by EPMA. in weight percent [wt%]

Sample	LLD (ppm)	31/5	31/6	66/6	66/7	90/1	90/6	92/3	92/6	103/3
Chemical composition (oxides wt%)										
CaO	500	55.5	54.1	54.0	55.5	55.2	55.3	55.4	56.0	53.6
SrO	270	0.0	0.0	0.0	0.0	0.0	0.0	0.0	0.0	0.0
Na ₂ O	340	0.2	0.0	0.1	0.2	0.2	0.2	0.1	0.2	0.1
Ce ₂ O ₃	900	0.3	0.4	0.2	0.5	0.3	0.4	0.4	0.2	0.4
La ₂ O ₃	2700	0.1	0.1	0.1	0.2	0.0	0.1	0.2	0.1	0.2
MnO	600	0.2	0.1	0.8	0.1	0.1	0.2	0.2	0.1	0.0
FeO	650	0.3	0.6	0.6	0.1	0.3	0.2	0.1	0.4	0.6
Y ₂ O ₃	900	0.4	0.3	0.6	0.3	0.5	0.5	0.4	0.2	0.9
Nd ₂ O ₃	950	0.3	0.4	0.2	0.4	0.2	0.4	0.4	0.3	0.6
P ₂ O ₅	450	42.3	40.8	41.2	42.6	42.3	42.0	41.8	42.3	40.3
SiO ₂	450	0.1	0.5	0.3	0.0	0.1	0.1	0.1	0.0	1.1
SO ₃	150	0.0	0.0	0.0	0.0	0.0	0.0	0.0	0.0	0.0
F	350	3.8	3.7	3.7	3.6	3.8	3.6	3.5	3.8	3.7
Cl	200	0.0	0.0	0.0	0.0	0.0	0.0	0.0	0.0	0.0
Total		103.97	103.02	103.15	101.85	103.06	102.85	102.66	103.82	101.37
-O(F)		1.60	1.58	1.60	1.52	1.58	1.53	1.49	1.60	1.56
-O(Cl)		0.01	0.00	0.00	0.00	0.00	0.01	0.00	0.00	0.00
Corrected sum		102.36	101.44	101.55	102.03	101.48	101.32	101.17	102.22	99.81
Atoms per formula unit [apfu]										
Ca		4.94	4.94	4.90	4.93	4.86	4.95	4.97	4.98	4.89
Sr		0.00	0.00	0.00	0.00	0.00	0.00	0.00	0.00	0.00
Na		0.03	0.00	0.02	0.03	0.03	0.03	0.02	0.03	0.02
Ce		0.01	0.01	0.01	0.02	0.01	0.01	0.01	0.01	0.01
La		0.00	0.00	0.00	0.01	0.00	0.00	0.01	0.00	0.01
Mn		0.01	0.01	0.06	0.01	0.01	0.01	0.01	0.01	0.00
Fe		0.02	0.04	0.04	0.01	0.02	0.01	0.01	0.03	0.04
Y		0.02	0.01	0.03	0.01	0.02	0.02	0.02	0.01	0.04
Nd		0.01	0.01	0.01	0.01	0.01	0.01	0.01	0.01	0.02
Msite		5.04	5.03	5.06	5.02	4.95	5.06	5.06	5.07	5.02
P		2.97	2.94	2.95	2.99	3.01	2.97	2.96	2.97	2.90
Si		0.01	0.04	0.03	0.00	0.01	0.01	0.01	0.00	0.09
S		0.00	0.00	0.00	0.00	0.00	0.00	0.00	0.00	0.00
Tsite		2.98	2.99	2.98	2.99	3.02	2.98	2.97	2.97	3.00
F		1.00	1.00	0.99	0.94	0.99	0.95	0.93	1.00	1.00
Cl		0.00	0.00	0.00	0.00	0.00	0.00	0.00	0.00	0.00
OH		0.00	0.00	0.01	0.06	0.01	0.05	0.07	0.00	0.00

Total number of complete analyses amounts to 54. Oxide contents recast into mineral composition formulae in apfu on the basis of twelve O

the presence of miarolitic pegmatite, which is characteristic of depths of 3–5 km, indicates pressures of 150–100 MPa (Janeczek 2007). The lowest pressure at which amphibole-bearing rocks can crystallize is in the range of 200–300 MPa (Maksimov 2009). The results of modelling using the equations proposed by Ridolfi et al. (2010)

revealed that the pressure during amphibole crystallization ranged from 223 ± 56 – 144 ± 36 MPa (Table 5). It can be noted that most of the amphibole crystals in our case study crystallized before biotite. Furthermore, these results appear to confirm and supplement those of previous studies.

Table 3 Estimation of crystallization conditions of apatite and coexisting melt composition

Sample	Apatite					T (°C)	F _{melt} (ppm)
	F (wt.%)	Cl (wt.%)	X (FAp)	X (ClAp)	F/Cl ratio		
31	3.71	0.02	1.95	0.01	414	892	2831
47	3.65	0.01	1.97	0.00	1078	910	2864
66	3.55	0.01	1.90	0.00	793	891	2750
67	3.73	0.01	1.98	0.00	2412	901	2877
90	3.56	0.00	1.92	0.00	2874	894	2780
92	3.74	0.01	1.99	0.00	415	894	2898
103	3.62	0.03	1.95	0.01	298	896	2824

Table 4 Main element oxide contents of selected amphibole grains from the SSM granitoids by EPMA, in weight percent [wt%]

Sample	LLD (ppm)	15/47	17/47	20/47	27/47	30/47	5/103	9/103	11/103	15/103
Chemical composition (oxides wt%)										
SiO ₂	170	40.9	41.0	41.1	41.2	41.3	41.2	41.4	40.2	41.1
TiO ₂	300	2.1	2.1	1.9	2.0	2.0	1.8	1.8	1.0	2.0
Al ₂ O ₃	150	8.7	8.7	8.6	8.7	8.6	8.6	8.5	8.5	8.7
Cr ₂ O ₃	400	0.0	0.0	0.0	0.0	0.0	0.0	0.0	0.0	0.0
FeO	650	26.4	26.6	26.7	26.3	26.0	26.3	27.4	29.3	26.1
MnO	550	0.5	0.4	0.5	0.5	0.5	0.8	0.5	1.1	0.5
MgO	150	4.6	4.5	4.6	4.7	4.7	4.6	4.4	3.2	4.7
CaO	250	10.3	10.2	10.1	10.3	10.3	10.1	10.3	10.2	10.4
Na ₂ O	200	1.9	2.0	2.1	2.0	2.1	2.0	1.9	1.9	2.0
K ₂ O	250	1.2	1.2	1.1	1.2	1.1	1.1	1.1	1.2	1.2
F	850	0.4	0.4	0.5	0.4	0.5	0.4	0.4	0.2	0.4
Cl	300	0.2	0.2	0.2	0.21	0.2	0.2	0.2	0.1	0.2
Total		97.21	97.35	97.48	97.62	97.493	97.14	98.02	96.83	97.48
-O(F)		0.16	0.16	0.22	0.18	0.22	0.16	0.19	0.10	0.18
-O(Cl)		0.04	0.05	0.05	0.05	0.05	0.05	0.06	0.02	0.06
Corrected sum		97.00	97.14	97.22	97.39	97.22	96.93	97.77	96.70	97.24
Atoms per formula unit [apfu]										
Si		6.48	6.49	6.49	6.50	6.54	6.51	6.51	6.44	6.51
Al ^{IV}		1.52	1.51	1.51	1.50	1.46	1.49	1.49	1.56	1.49
Ti		0.00	0.00	0.00	0.00	0.00	0.00	0.00	0.00	0.00
Tsite		8.00	8.00	8.00	8.00	8.00	8.00	8.00	8.00	8.00
Al ^{VI}		0.10	0.11	0.10	0.12	0.14	0.12	0.09	0.04	0.13
Ti		0.25	0.25	0.23	0.24	0.24	0.21	0.21	0.12	0.24
Cr		0.00	0.00	0.00	0.00	0.00	0.00	0.00	0.00	0.00
Fe ³⁺		0.60	0.58	0.67	0.57	0.48	0.68	0.71	0.94	0.50
Mg		1.09	1.06	1.08	1.11	1.11	1.08	1.03	0.76	1.11
Fe ²⁺		2.89	2.94	2.85	2.90	2.96	2.79	2.90	2.98	2.95
Mn		0.07	0.05	0.07	0.07	0.07	0.11	0.07	0.15	0.07
Csite		5.00	5.00	5.00	5.00	5.00	5.00	5.00	5.00	5.00
Fe ²⁺		0.00	0.00	0.00	0.00	0.00	0.00	0.00	0.00	0.00
Ca		1.75	1.73	1.71	1.74	1.75	1.71	1.74	1.75	1.76
Na		0.25	0.27	0.29	0.26	0.25	0.29	0.26	0.25	0.24
Bsite		2.00	2.00	2.00	2.00	2.00	2.00	2.00	2.00	2.00
Na		0.33	0.34	0.35	0.35	0.39	0.32	0.31	0.34	0.38
K		0.24	0.24	0.22	0.24	0.22	0.22	0.22	0.25	0.24
A site		0.57	0.59	0.57	0.59	0.61	0.55	0.54	0.59	0.62
		15.57	15.59	15.57	15.59	15.61	15.55	15.54	15.59	15.62
F		0.20	0.20	0.25	0.20	0.25	0.20	0.20	0.10	0.20
Cl		0.05	0.05	0.05	0.06	0.05	0.05	0.05	0.03	0.05
OH		1.75	1.75	1.70	1.74	1.70	1.75	1.75	1.87	1.75

FeO represents total iron oxide content. OH calculated by balance to 100.00 wt%. Total number of complete analyses amounts to 45. Oxide contents recast into mineral composition formulae in apfu on the basis of twenty-three O

Burnham (1979) observed that hornblende is stable in magmas containing >3 wt.% H₂O, which implies that the hornblende-biotite granite crystallized from a magma that was enriched in water Puziewicz (1990). The results obtained using the equation of Holtz et al. (2001) indicate that the water content was even greater, ranging from 6.5 - 5.5 wt. % (Table 5). This value is close to the upper limit of the water content at which amphibole is stable (Fig. 4). It must be noted that the model used for these calculations is dedicated to rhyolitic melts; therefore, it is suitable for this investigation, and the obtained results can be considered to be reliable. Previous studies based on observations of miarolitic pegmatites also indicated water-rich magmas (Janeczek 1985).

Table 5 Estimation of crystallization conditions of amphibole and volatile contents of coexisting melt

Sample	47			103		
	Min	Max	Average	Min	Max	Average
F (wt. %)	0.32	0.45	0.40	0.18	0.51	0.37
Cl (wt. %)	0.18	0.24	0.21	0.16	0.25	0.21
Mg#	0.21	0.24	0.23	0.16	0.24	0.23
F/Cl ratio	2.70	4.26	3.55	1.49	5.11	3.37
T (°C)	796	829	813	768	818	803
uncertainty (σ_{est})	22	22	22	22	22	22
P (MPa)	178	223	196	144	209	188
uncertainty (max error)	44	56	49	36	52	47
H ₂ O _{melt} (wt.%)	5.5	6.2	5.8	5.7	6.5	6.1
uncertainty (σ_{est})	0.4	0.9	0.7	0.4	0.9	0.6
OH (mol %)	10.3	11.4	10.9	10.6	11.8	11.2
Cl _(ppm)	1095	1494	1282	901	1468	1230
F _(ppm)	1819	2963	2435	919	2991	2172

Table 6 Main element oxide contents of selected biotite grains from the SSM granitoids by EPMA. in weight percent [wt%]

Sample	LLD (ppm)	32/9	47/78	47/90	66/01	66/06	66/80	66/81	67/01	90/02	90/03	90/04
Chemical composition (oxides wt%)												
SiO ₂	450	34.4	34.2	34.3	34.5	34.6	35.0	34.3	34.3	34.9	34.5	34.4
TiO ₂	2400	3.9	3.4	3.6	3.9	3.7	3.9	3.7	3.3	3.4	3.8	3.6
Al ₂ O ₃	350	13.6	13.6	13.9	13.4	13.6	13.9	13.4	12.8	12.7	12.9	12.9
Cr ₂ O ₃	850	0.0	0.1	0.0	0.0	0.0	0.0	0.0	0.0	0.0	0.02	0.0
MgO	350	5.0	5.2	5.2	5.2	5.1	5.1	5.2	4.0	4.2	3.8	4.1
CaO	600	0.0	0.0	0.0	0.0	0.0	0.0	0.0	0.0	0.0	0.0	0.0
MnO	700	0.4	0.3	0.5	0.7	0.6	0.4	0.3	0.6	0.5	0.6	0.5
FeO	700	28.2	29.0	28.5	28.0	28.4	28.6	29.6	31.2	29.8	31.0	30.7
BaO	500	0.0	0.0	0.0	0.0	0.0	0.0	0.0	0.0	0.0	0.0	0.0
K ₂ O	550	9.4	9.3	9.3	9.3	9.4	9.4	9.2	9.0	9.3	9.4	9.4
F	600	0.2	0.3	0.5	0.1	0.1	0.5	0.2	0.2	0.3	0.6	0.1
Cl	800	0.1	0.1	0.1	0.2	0.3	0.3	0.1	0.1	0.1	0.2	0.2
Total		95.31	95.46	96.00	95.27	95.81	97.14	96.03	95.51	95.41	96.73	95.90
-O(F)		0.09	0.12	0.21	0.05	0.06	0.19	0.07	0.06	0.13	0.24	0.03
-O(Cl)		0.02	0.02	0.02	0.05	0.06	0.07	0.02	0.03	0.03	0.04	0.04
Corrected sum		95.20	95.31	95.77	95.16	95.69	96.89	95.94	95.42	95.25	96.46	95.83
Atoms per formula unit [apfu]												
Si ^(IV)		5.56	5.54	5.53	5.57	5.57	5.57	5.53	5.61	5.69	5.60	5.60
Al ^(IV)		2.44	2.46	2.47	2.43	2.43	2.43	2.47	2.39	2.31	2.40	2.40
Tsite		8.00	8.00	8.00	8.00	8.00	8.00	8.00	8.00	8.00	8.00	8.00
Al ^(VI)		0.15	0.13	0.17	0.12	0.15	0.17	0.07	0.08	0.13	0.06	0.07
Ti		0.47	0.41	0.44	0.47	0.45	0.47	0.45	0.41	0.42	0.46	0.44
Fe ⁺²		3.81	3.93	3.84	3.78	3.82	3.80	3.99	4.27	4.06	4.20	4.18
Mn		0.05	0.04	0.07	0.10	0.08	0.05	0.04	0.08	0.07	0.08	0.07
Mg		1.21	1.26	1.25	1.25	1.22	1.21	1.25	0.98	1.02	0.92	0.99
Ca		0.00	0.00	0.00	0.00	0.00	0.00	0.00	0.00	0.00	0.00	0.00
Osite		5.70	5.77	5.76	5.72	5.73	5.71	5.80	5.81	5.70	5.73	5.75
K		1.94	1.92	1.91	1.92	1.93	1.91	1.89	1.88	1.93	1.95	1.95
Asite		1.94	1.92	1.91	1.92	1.93	1.91	1.89	1.88	1.93	1.95	1.95
		15.64	15.69	15.67	15.64	15.66	15.62	15.70	15.69	15.64	15.68	15.70
F		0.01	0.01	0.02	0.00	0.00	0.02	0.01	0.01	0.01	0.03	0.00
Cl		0.00	0.00	0.00	0.00	0.00	0.00	0.00	0.00	0.00	0.00	0.00
OH		1.99	1.99	1.98	1.99	1.99	1.97	1.99	1.99	1.99	1.97	1.99

FeO represents total iron oxide content. BaO contents for all grains under LLD. OH calculated by balance to 100.00 wt%. Total number of complete analyses amounts to 45. Oxide contents recast into mineral composition formulae in apfu on the basis of twenty-three O

The issue of the SSM crystallization temperature is as problematic as that of its pressure. The TZr values of the hornblende-biotite granite range from 749 - 860 °C, with an average value of 804 °C; in principle, this is the highest for the whole massif. Because there are most likely no inherited zircons in these rocks, this represents a minimum TZr temperature. (Turniak et al. 2014). Most granitic melts that are unsaturated in water crystallize at temperatures of 900-850 °C, whereas their water-rich equivalents form at temperatures that are approximately 100-200 °C lower (Puziewicz 1990). It has been

experimentally proven that biotite in water saturated conditions is stable up to the temperature of 810 °C in granitic melts. In contrast, in under-saturated in water conditions, it disappears at a temperature exceeding approximately 830 °C (Puziewicz and Johannes 1990). On the contrary, biotite is stable up until the complete solidification of the rock, which occurs at a temperature of approximately 680 °C (Naney 1983). Since there is no geothermometer that is suitable for crystallization temperature calculation of biotites in water-saturated granitic melts, solidification temperature proposed by Naney

Table 7 Estimation of crystallization conditions of biotite and coexisting melt composition.

Sample	Biotite					T° (°C)	Melt		
	Ti (pfu)	Mg#	log(F/OH)	log(Cl/OH)	F/Cl ratio		F (ppm)	Cl (ppm)	
								$D_C^{Bt/E} = 2.97$	$D_C^{Bt/E} = 6.25$
31	0.452	0.275	-2.25	-2.99	5.32	680	1997	571	272
47	0.438	0.206	-2.37	-3.11	7.26	680	2940	430	204
66	0.381	0.183	-2.32	-3.26	8.98	680	3135	301	143
67	0.392	0.188	-2.32	-3.13	10.26	680	2995	401	190
90	0.392	0.183	-2.35	-3.12	4.59	680	2996	405	192
92	0.458	0.175	-2.11	-3.23	8.65	680	3085	321	153
103	0.475	0.192	-2.54	-3.00	7.96	680	2469	532	253

° Solidification temperature according to Naney (1983)

(1983) has been used in calculations. Hornblende crystallization occurs in naturally occurring granitic magmas at temperatures of less than c. 810 °C (Dall'agnol et al. 1999). The crystallization temperatures of amphibole from the hornblende-biotite granite of the SSM obtained using the equation proposed by Ridolfi et al. (2010) range from 768–829 °C, with an error of 22 °C. According to Bowen's reaction series, apatite is one of the first minerals that crystallize in magma, at temperatures exceeding 900 °C, i.e., 900–924, according to Webster et al. (2009). The Apatite Saturation Temperatures (ASTs) calculated for apatite from the SSM (Harrison and Watson 1984) range from 910–892 °C (Table 1). It must be noted that by volume, most apatite in magmatic environments, from mafic to felsic, crystallizes in a narrow temperature interval below the AST (Piccoli and Candela 2002).

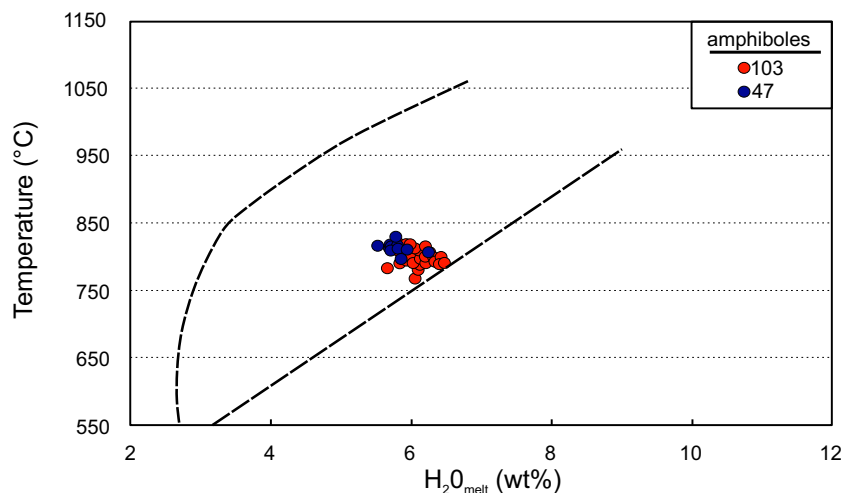
Evolution of Cl and F concentrations during crystallization of the SSM

Some studies have been performed on concentrations of volatiles that depend on the composition of the magma (e.g., Shabani et al. 2003; De De Vivo et al. 2005; Wallace 2005; Teiber et al.

2014; Zellmer et al. 2015; Bao et al. 2016). Unfortunately, this information is lacking in the Variscan granitoids. Rocks of the hornblende-biotite variety of SSM granite are characterized by a high initial $^{87}\text{Sr}/^{86}\text{Sr}$ ratio, which indicates that the continental crust is their main protolith, and their silica contents range from 72.09–75.62 wt.%. Concentrations of F in the melts are dependent on the agpaite index ((Na+K)/Al). Therefore, granitic rocks exhibiting metaluminous characteristics (i.e., $(Na + K)/Al < 1$) should rather have the lowest concentrations of F (Scaillet and Macdonald 2004). The hornblende-biotite granite rocks of the SSM are not exceptions to this rule. Their agpaite index values range from 0.75 to 0.81 (Domańska-Siuda 2007).

Since previous researchers have proposed that limited magma mixing occurred in the SSM (Domańska-Siuda and Slaby 2003, 2004, 2005; Domańska-Siuda 2007), the influence of volatiles from mafic melt is expected to be limited. Unfortunately, most research related to volatiles in magmatic systems have focused on volatiles in subduction zones (e.g., De De Vivo et al. 2005, Wallace 2005, Zellmer et al. 2015). The concentrations of halogens vary widely in mafic and intermediate melts. Nevertheless, mafic melts generally seem to have lower F and higher Cl concentrations than crustal melts (Teiber et al. 2014). Therefore,

Fig. 4 Estimated water contents in magmas from the SSM using equation and plot by Ridolfi et al. (2010). Dashed lines represent range of amphibole stability conditions



volatile-bearing minerals, e.g., apatite, can be used to estimate the sources of both volatiles and magmas. Furthermore, they can be used to determine the mechanism of magma evolution. The Cl contents in apatite crystals from Irazú volcano, Costa Rica, ranged from 5000 ppm to 20,000 ppm, and their F contents ranged from 24,000 ppm to 37,000 ppm. These variations were interpreted using experimental partitioning data, which indicated that the changing abundances of these volatiles in the melt were due to magma mixing and degassing (Boyce and Hervig 2009). Calculations made for apatite from the Plinian phase of the Bishop Tuff suggested that the initial melt contained 960–700 ppm Cl and 300–160 ppm F (Piccoli and Candela 1994). Furthermore, the fluorine concentration calculated from the apatite-saturated lavas of the 2006 eruption of Augustino volcano, Alaska (USA), is 40 ppm, whereas its apatite crystals contain 2.2 wt.% F. Melt inclusions from this eruption record F concentrations of ~200–300 ppm and 3300–3800 ppm Cl (Webster and Piccoli 2015). Moreover, calculations made from apatite from diorite and gabbro of the Liujiawa pluton in the Dabie orogeny, China, indicate much higher F concentrations of 2000–3000 ppm and approx. 1,000 ppm Cl. Additionally, the concentrations of Cl and F calculated from its amphiboles were 1000–2000 and 2000–3000 ppm, respectively, whereas the concentrations calculated based on volatiles in biotite crystals yielded results of ~400 ppm F and ~1200 ppm Cl (Zhang et al. 2012).

Our research allowed us to derive F concentrations from apatite, amphibole and biotite and consequently to estimate its evolution path during melt crystallization. The F concentrations in the melt range from ~2000–3000 ppm and do not change significantly within the crystallization interval. Most likely, the first interval (Fig. 5a) was controlled by mineral crystallization in a system that was closed with respect to F. Since apatite contributes less than 30% of F in the granitic rock budget (Teiber et al. 2014), its crystallization should change the halogen composition only marginally. The next crystallization interval (Fig. 5a), as recorded by amphibole and biotite, also does not indicate that changes occurred in the F concentration of the melt. Since biotite controls up to

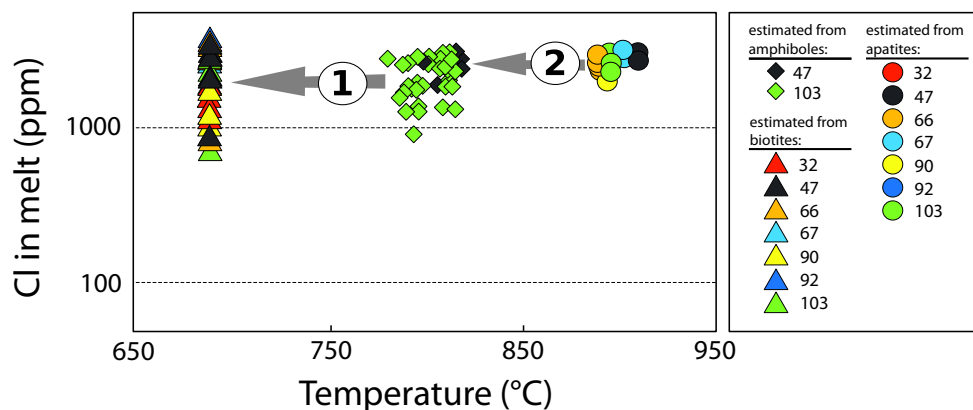
75 wt.% of F in the granitic rock budget (Teiber et al. 2014), its crystallization might cause a major decrease in the fluorine concentration of the melt. On the other hand, the crystallization of F-free minerals, e.g., feldspar and quartz, would lead to an increase in the F concentration of the melt. Most likely, both processes compensated for each other. Furthermore, it is known that silicate melt accommodates F more readily than aqueous fluid, and the concentration of F in the melt during crystallization was relatively constant (Zhang et al. 2012).

As illustrated in Fig. 6, Cl concentrations were estimated based on the compositions of amphibole and biotite. Values calculated from amphibole range from 1470–900 ppm, whereas those calculated from biotite range from 1000–100 ppm. The crystallization interval shows the decrease in the Cl concentration of the melt (Fig. 6a). This feature can also be explained by the continuous exsolution of aqueous fluid from a silicate melt. This explanation was proposed for the decreased Cl concentrations in the melt of the Liujiawa pluton (Zhang et al. 2012). Secondly, because biotite controls up to 90 wt.% of Cl in the rock budget (Teiber et al. 2014), its crystallization might cause the chlorine concentration in the melt to decrease. Furthermore, as noted by previous researchers (e.g., Zhang et al. (2012)), the effect of the strong control of pressure on the estimation of Cl concentrations in the melt is visible in Fig. 6b.

Magma mixing

The F/Cl ratios in volatile-bearing minerals can be used as indicators of the magma source (Teiber et al. 2014). Relatively evolved granites have high F/Cl ratios. In contrast, amphibole-bearing granites, granodiorites, monzonites and diorites have lower F and higher Cl concentrations and therefore have lower F/Cl ratios. Since F and Cl are similarly incompatible, the F/Cl ratio should not change substantially during crystallization (Zhang et al. 2012; Teiber et al. 2014). In the investigated samples, the F/Cl ratios can be used to identify the contribution of a mafic and/or mantle-derived component from a generally crustal metasedimentary source. Figure 7 shows the changes in the F/Cl ratios of apatite, amphibole

Fig. 5 F concentrations in melt estimated from mineral compositions as functions of temperature for the Strzegom-Sobótka granite



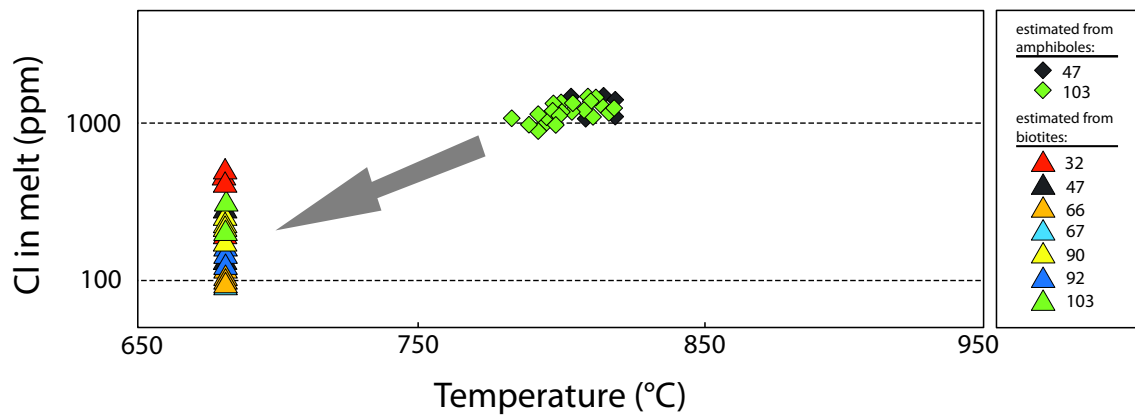


Fig. 6 Cl concentrations in melt estimated from mineral compositions as functions of temperature for the Strzegom-Sobótka granite

and biotite during crystallization. Significant changes in these values between apatite and amphibole (Fig. 7) are noticeable. These changes were most likely caused by the delivery of chlorine from a Cl-rich source while the system was open. Since mantle-delivered compounds are expected to be Cl-rich, they are most likely responsible for the delivery of Cl into the system. Previous researchers (Domańska-Siuda and Słaby 2003, 2004, 2005) have noted that the volume of mafic melt that mixed with the granitic melt was insignificant. Nevertheless, even a small quantity of such material containing a relatively large amount of Cl could dramatically change the F/Cl ratios of the melt. Furthermore, the injection of a small volume of F-poor material should change the F concentrations of the melt only marginally (Fig. 5a). This episode was recorded by changes in the F/Cl ratios between apatite and amphibole (Fig. 7). Mafic material was injected while the melt was crystallizing; therefore, fluctuations in the composition of volatiles might be used as indicators of the delivery of new melt. Later, the values of the F/Cl ratio did not change during the interval of amphibole and biotite crystallization (Fig. 7), which might be explained by the crystallization of magma.

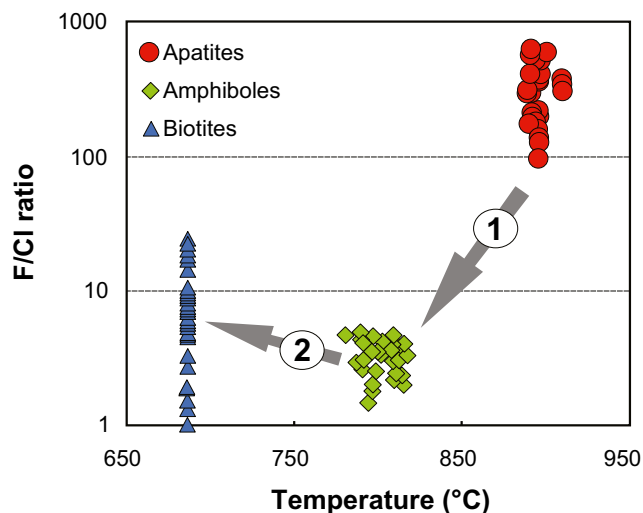


Fig. 7 F/Cl ratios calculated from apatite, amphibole and biotite

Conclusions

Volatile-bearing minerals can be used to estimate the origin, sources and evolutionary paths of melts. Furthermore, they can provide information about melt injections that can cause significant or limited hybridization. The granites of the SSM are no exception to this rule. The origin of the SSM is associated with the occurrence of widespread bimodal volcanism across the Sudetes Mountains and the northern Variscan foreland, and it was caused by the progressive input of heat into the crust contributed from ascending basaltic magmas. Previous authors have used petrographic and geochemical evidence to suggest that the SSM is a product of fractional crystallization and limited magma mixing (Domańska-Siuda and Słaby 2003, 2004, 2005). The melts from which the SSM crystallized are generally crustal, yet they record the minor influence of mantle-delivered compounds, especially in the case of the hornblende-biotite variety. Furthermore, the influence of the lithospheric mantle is mostly limited to thermal influx into the lower crust, which consequently caused its melting. This study notes that evolution of SSM consisted of couple of phases:

1. The melting of continental crust that was caused by heat from basaltic magma. During this phase the system was closed, and there is no evidence of the influence of any mafic components. It was recorded by the volatile composition of apatite.
2. Delivery of small quantity of mafic material into the crystallizing melt by ascending basaltic magma. It occurred between the crystallization of apatite and amphibole and was recorded by dramatic changes in the F/Cl ratios of both minerals.
3. Crystallization of amphibole in closed magmatic system.
4. Reopen of the system. It has been recorded by the volatile composition of biotite. Concentration of Cl in the melt decreased during this phase. This was most likely caused by the exsolution of aqueous fluid from the silicate melt.

Open Access This article is distributed under the terms of the Creative Commons Attribution 4.0 International License (<http://creativecommons.org/licenses/by/4.0/>), which permits unrestricted use, distribution, and reproduction in any medium, provided you give appropriate credit to the original author(s) and the source, provide a link to the Creative Commons license, and indicate if changes were made.

References

- Aiuppa A, Baker DR, Webster JD (2009) Halogens in volcanic systems. *Chem Geol* 263:1–18
- Aleksandrowski P, Kryza R, Mazur S, Zaba J (1997) Kinematic data on major Variscan strike-slip faults and shear zones in the Polish Sudetes, northeast Bohemian Massif. *Geol Mag* 134:727–739
- Awdankiewicz M, Awdankiewicz H, Kryza R et al (2010) SHRIMP zircon study of a micromonzodiorite dyke in the Karkonosze Granite, Sudetes (SW Poland): Age constraints for late Variscan magmatism in Central Europe. *Geol Mag* 147(1):77–85
- Baker DR, Freda C, Brooker RA, Scarlato P (2005) Volatile diffusion in silicate melts and its effects on melt inclusions. *Ann Geophys* 48: 699–717
- Bao B, Webster JD, Zhang DH et al (2016) Compositions of biotite, amphibole, apatite and silicate melt inclusions from the Tongchang mine, Dexing porphyry deposit, SE China: Implications for the behavior of halogens in mineralized porphyry systems. *Ore Geol Rev* 79:443–462
- Barbarin B (1999) A review of the relationships between granitoid types, their origins and their geodynamic environments. *Lithos* 46:605–626
- Borkowska M (1957) Granitoidy kudowskie na tle petrografii głównych typów kwaśnych intruzji Sudetów i ich przedpola. *Arch Mineral* 21: 229–379
- Boyce JW, Hervig RL (2009) Apatite as a monitor of late-stage magmatic processes at Volcan Irazu, Costa Rica. *Contrib to Mineral Petrol* 157: 135–145
- Brueckner HK, Blusztajn J, Bakun-Czubarow N (1996) Trace element and Sm-Nd “age” zoning in garnets from peridotites of the Caledonian and Variscan Mountains and tectonic implications. *J Metamorph Geol* 14:61–73
- Burnham CW (1979) Magmas and hydrothermal fluids. In: Barnes HL (ed) *Geochemistry of Hydrothermal Ore Deposits*, 2nd edn. John Wiley and Sons, New York, pp 71–136
- Coulson IM, Dipple GM, Raudsepp M (2001) Evolution of HF and HCl activity in magmatic volatiles of the gold-mineralized Emerald Lake pluton, Yukon Territory, Canada. *Miner Depos* 36:594–606
- Dall’agnol R, Scaillet B, Pichavant M (1999) An Experimental Study of a Lower Proterozoic A-type Granite from the Eastern Amazonian Craton, Brazil. *J Petrol* 40:1673–1698
- De Vivo B, Lima A, Webster JD (2005) Volatiles in Magmatic-Volcanic Systems. *Elements* 1:19–24
- Domańska-Siuda J (2007) The granitoid Variscan Strzegom-Sobótka massif. In: Kozłowski A, Wiszniewska J (eds) *Granitoids in Poland*, AM Monograph No. 1. KNM PAN-WG UW, pp 179–199
- Domańska-Siuda J, Słaby E (2003) Enclaves from the variscan Strzegom-Sobótka hornblende-biotite granite. *Mineral Soc Pol – Spec Pap* 23: 57–59
- Domańska-Siuda J, Słaby E (2004) The hornblende-biotite granite from Strzegom-Sobótka Massif – parental magma evolution. *Mineral Soc Pol – Spec Pap* 24:131–134
- Domańska-Siuda J, Słaby E (2005) One-sided contamination of lamprophyric melt drops in hornblende-biotite granite magma chamber - a case study of Strzegom Massif. *Mineral Soc Pol – Spec Pap* 25:67–70
- Finch AA, Parsons I, Mingard SC (1995) Biotites as Indicators of Fluorine Fugacities in Late-Stage Magmatic Fluids: the Gardar Province of South Greenland. *J Petrol* 36:1701–1728
- Harlov DE, Forster H-J (2002) High-Grade Fluid Metasomatism on both a Local and a Regional Scale: the Seward Peninsula, Alaska, and the Val Strona di Omegna, Ivrea-Verbanò Zone, Northern Italy. Part I: Petrography and Silicate Mineral Chemistry. *J Petrol* 43:769–799
- Harrison TM, Watson EB (1984) The behavior of apatite during crustal anatexis: equilibrium and kinetic considerations. *Geochim Cosmochim Acta* 48:1467–1477
- Hawthorne FC, Oberti R, Harlow GE et al (2012) IMA Report – Nomenclature of the amphibole supergroup. *Am Miner* 97:2031–2048
- Hedenquist JW, Lowenstern JB (1994) The role of magmas in the formation of hydrothermal ore deposits. *Nature* 370:519–527
- Holdaway MJ (1971) Stability of andalusite and the aluminum silicate phase diagram. *Am J Sci* 271:97–131
- Holtz F, Johannes W, Tamic N, Behrens H (2001) Maximum and minimum water contents of granitic melts generated in the crust: A re-evaluation and implications. *Lithos* 56:1–14
- Huston DL, Relvas JMRS, Gemmel JB, Driberg S (2011) The role of granites in volcanic-hosted massive sulphide ore-forming systems: An assessment of magmatic-hydrothermal contributions. *Miner Depos* 46:473–507
- Icenhower J, London D (1995) An experimental study of element partitioning among biotite, muscovite, and coexisting peraluminous silicic melt at 200 MPa (H₂O). *Am Mineral* 80:1229–1251
- Icenhower JP, London D (1997) Partitioning of fluorine and chlorine between biotite and granitic melt: experimental calibration at 200 MPa H₂O. *Contrib to Mineral Petrol* 127:17–29
- Janeček J (1985) Typomorphic minerals of pegmatites from the Strzegom-Sobótka granitic massif. *Geol Sudetica* 20:1–63
- Janeček J (2007) Intragranitic pegmatites of the Strzegom-Sobótka massif – an overview. In: Kozłowski A, Wiszniewska J (eds) *Granitoids in Poland*, AM Monograph No. 1. KNM PAN-WG UW, pp 193–201
- Kröner AEH (1998) Geochemistry, single zircon ages and Sm-Nd systematics of granitoid rocks from the Góry Sowie Block (Owl Mts), Polish West Sudetes: evidence for early Paleozoic arc-related plutonism. *J Geol Soc London* 155:711–724
- Kryza R, Pin C (2002) Mafic rocks in a deep-crustal segment of the Variscides (the Góry Sowie, SW Poland): Evidence for crustal contamination in an extensional setting. *Int J Earth Sci* 91:1017–1029
- Kural S, Morawski T (1968) Strzegom-Sobótka granitic massif. *Biul Inst Geol* 27:33–74
- Maciejewski S, Morawski T (1970) Wstępne wyniki badań petrograficznych strzegomskiego masywu granitowego. *Kwart Geol* 14:885–887
- Maciejewski S, Morawski T (1975) Zmienność petrograficzna granitów masywu strzegomskiego. *Kwart Geol* 19:47–65
- Majerowicz A (1972) Masyw granitowy Strzegom-Sobótka. *Geol Sudetica* 6:7–96
- Maksimov AP (2009) The influence of water on the temperature of amphibole stability in melts. *J Volcanol Seismol* 3:27–33
- Mason RA (1992) Models of order and iron-fluorine avoidance in biotite. *Can Mineral* 30:343–354
- Mathez EA, Webster JD (2005) Partitioning behavior of chlorine and fluorine in the system apatite-silicate melt-fluid. *Geochim Cosmochim Acta* 69:1275–1286
- Mikulski SZ, Stein HJ (2005) Re-Os age for molybdenite from the Variscan Strzegom-Sobótka massif, SW Poland. In: Mao J, Bierlein FP (eds) *Mineral deposit research: meeting the global challenge*. Springer, Berlin Heidelberg, pp 789–792
- Mungall JE, Brennan JM, Godel B et al (2015) Transport of metals and sulphur in magmas by flotation of sulphide melt on vapour bubbles. *Nat Geosci* 8:216–219

- Munoz JL (1984) F-OH and Cl-OH exchange in micas with applications to hydrothermal ore deposits. *Rev Mineral Geochemistry* 13:469–493
- Munoz JL (1992) Calculation of HF and HCl fugacities from biotite compositions: revised equations. In: vol 26. Geological Society of America, Abstracts with Programs. p A221
- Naney MT (1983) Phase equilibria of rock-forming ferromagnesian silicates in granitic systems. *Am J Sci* 283:993–1033
- Nowak M, Behrens H (2001) Water in rhyolitic magmas: Getting a grip on a slippery problem. *Earth Planet Sci Lett* 184:515–522
- Oliver GJH, Corfu F, Krogh TE (1993) U-Pb ages from SW Poland: evidence for a Caledonian suture zone between Baltica and Gondwana. *J Geol Soc London* 150:355–369
- Pasero M, Kampf AR, Ferraris C et al (2010) Nomenclature of the apatite supergroup minerals. *Eur J Mineral* 22:163–179
- Piccoli P, Candela P (1994) Apatite in felsic rocks: a model for the estimation of initial halogen concentrations in the Bishop Tuff (Long Valley) and Tuolumne Intrusive Suite (Sierra Nevada batholith) magmas. *Am J Sci* 294:92–135
- Piccoli PM, Candela PA (2002) Apatite in igneous systems. *Rev Mineral Geochemistry* 48:255–292
- Piccoli PM, Candela PA, Williams TJ (1999) Estimation of aqueous HCl and Cl concentrations in felsic systems. *Lithos* 46:591–604
- Pichavant M, Manning D (1984) Petrogenesis of tourmaline granites and topaz granites; the contribution of experimental data. *Phys Earth Planet Inter* 35:31–50
- Pin C, Puziewicz J, Duthou J-L (1988) Studium izotopowe Rb-Sr oraz Sm-Nd masywu granitowego Strzegom-Sobótka. In: *Petrologia i geologia fundamentu waryscyjskiego polskiej części Sudetów*. pp 37–41
- Pin C, Puziewicz J, Duthou J-L (1989) Ages and origins of a composite granitic massif in the Variscan belt: a Rb-Sr study of the Strzegom-Sobótka Massif, W. Sudetes (Poland). *Neues Jahrb für Mineral - Abhandlungen* 160:71–82
- Puziewicz J (1981) Andalusite tourmaline aplite from Lisiec Hill near Strzegom. *Mineral Pol* 12:69–76
- Puziewicz J (1985) *Petrologia skał masywu granitowego Strzegom-Sobótka*. In: *Petrologia skał masywu granitowego Strzegom-Sobótka i jego osłony*. pp 19–27
- Puziewicz J (1990) Masyw granitowy Strzegom-Sobótka. Aktualny stan badań. *Arch Mineral* 45:135–154
- Puziewicz J, Johannes W (1990) Experimental study of a biotite-bearing granitic system under water-saturated and water-undersaturated conditions. *Contrib to Mineral Petrol* 104:397–406
- Ridolfi F, Renzulli A, Puerini M (2010) Stability and chemical equilibrium of amphibole in calc-alkaline magmas: An overview, new thermobarometric formulations and application to subduction-related volcanoes. *Contrib to Mineral Petrol* 160:45–66
- Sato H, Holtz F, Behrens H et al (2005) Experimental petrology of the 1991-1995 Unzen dacite, Japan. Part II: Cl/OH partitioning between hornblende and melt and its implications for the origin of oscillatory zoning of hornblende phenocrysts. *J Petrol* 46:339–354
- Scailliet B, Macdonald R (2004) Fluorite stability in silicic magmas. *Contrib to Mineral Petrol* 147:319–329
- Shabani AAT, Lalonde AE, Whalen JB (2003) Composition of biotite from granitic rocks of the Canadian Appalachian orogen: A potential tectonomagmatic indicator? *Can Mineral* 41:1381–1396
- Słaby E, Koch-Müller M, Förster H-J et al (2016) Determination of volatile concentrations in fluorapatite of Martian shergottite NWA 2975 by combining synchrotron FTIR, Raman spectroscopy, EMPA, and TEM, and inferences on the volatile budget of the apatite host-magma. *Meteorit Planet Sci* 51:1–17
- Stormer JC, Pierson ML, Tacker RC (1993) Variation of F and Cl X-ray intensity due to anisotropic diffusion in apatite during electron microprobe analysis. *Am Min* 78:641–648
- Teiber H, Marks MAW, Wenzel T et al (2014) The distribution of halogens (F, Cl, Br) in granitoid rocks. *Chem Geol* 374–375:92–109
- Turniak K, Tichomirowa M, Bombach K (2005) Zircon Pb-evaporation ages of granitoids from the Strzegom-Sobótka massif (SW Poland). *Mineral Soc Pol – Spec Pap* 25:241–245
- Turniak K, Halas S, Wójtowicz A (2007) New K-Ar Cooling Ages of Granitoids from the Strzegom-Sobótka Massif, SW Poland. *Geochronometria* 27:5–9
- Turniak K, Mazur S, Domańska-Siuda J, Szuszkiewicz A (2014) SHRIMP U-Pb zircon dating for granitoids from the Strzegom-Sobótka Massif, SW Poland: Constraints on the initial time of Permo-Mesozoic lithosphere thinning beneath Central Europe. *Lithos* 208:415–429
- Wallace PJ (2005) Volatiles in subduction zone magmas: Concentrations and fluxes based on melt inclusion and volcanic gas data. *J Volcanol Geotherm Res* 140:217–240
- Webster JD, Piccoli PM (2015) Magmatic Apatite: A Powerful, Yet Deceptive, Mineral. *Elements* 11:177–182
- Webster JD, Tappen CM, Mandeville CW (2009) Partitioning behavior of chlorine and fluorine in the system apatite-melt-fluid. II: Felsic silicate systems at 200 MPa. *Geochim Cosmochim Acta* 73:559–581
- Whitney JA (1988) The origin of granite: The role and source of water in the evolution of granitic magmas. *Geol Soc Am Bull* 100:1886–1897
- Whitney DL, Evans BW (2010) Abbreviations for names of rock-forming minerals. *Am Min* 95:185–187
- Wilson M, Neumann E-R, Davies GR et al (2004) Permo-Carboniferous magmatism and rifting in Europe: introduction. *Geol. Soc. Spec. Publ* 223:1–10
- Zellmer GF, Edmonds M, Straub SM (2015) Volatiles in subduction zone magmatism. *Geol Soc London, Spec Publ* 410:1–17
- Zhang C, Holtz F, Ma C et al (2012) Tracing the evolution and distribution of F and Cl in plutonic systems from volatile-bearing minerals: A case study from the Liujiawa pluton (Dabie orogen, China). *Contrib to Mineral Petrol* 164:859–879
- Zhu C, Sverjensky DA (1991) Partitioning of F-Cl-OH between minerals and hydrothermal fluids. *Geochim Cosmochim Acta* 55:1837–1858
- Zhu C, Sverjensky DA (1992) F-Cl-OH partitioning between biotite and apatite. *Geochim Cosmochim Acta* 56:3435–3467